ISSN 0020-1685, Inorganic Materials, 2020, Vol. 56, No. 12, pp. 1242–1247. © Pleiades Publishing, Ltd., 2020.
Russian Text © The Author(s), 2020, published in Neorganicheskie Materialy, 2020, Vol. 56, No. 12, pp. 1311–1316.

Synthesis, Crystal Structure and Thermodynamic Properties of $LuGaTi_2O_7$

L. T. Denisova[a, *], M. S. Molokeev[a, b], L. G. Chumilina[a], Yu. F. Kargin[c], V. M. Denisov[a], and V. V. Ryabov[d]

[a] *Siberian Federal University, Krasnoyarsk, 660041 Russia*
[b] *Kirensky Institute of Physics, Krasnoyarsk Scientific Center (Federal Research Center), Siberian Branch, Russian Academy of Sciences, Krasnoyarsk, 660036 Russia*
[c] *Baikov Institute of Metallurgy and Materials Science, Russian Academy of Sciences, Moscow, 119991 Russia*
[d] *Institute of Metallurgy, Ural Branch, Russian Academy of Sciences, Yekaterinburg, 620016 Russia*
**e-mail: ldenisova@sfu-kras.ru*

Received June 14, 2020; revised August 6, 2020; accepted August 10, 2020

Abstract—Single-phase $LuGaTi_2O_7$ samples have been prepared by solid-state reaction in a starting mixture of Lu_2O_3, Ga_2O_3, and TiO_2 via sequential firing in air at temperatures of 1273 and 1573 K. The crystal structure of the lutetium gallium dititanate has been determined by the Rietveld method (profile analysis of X-ray diffraction patterns of polycrystalline powders): sp. gr. *Pcnb*; a = 9.75033(13) Å, b = 13.41425(17) Å, c = 7.29215(9) Å, V = 957.32(2) Å^3, d = 6.28 g/cm^3. The heat capacity of $LuGaTi_2O_7$ has been determined as a function of temperature by differential scanning calorimetry in the range 320–1000 K. The $C_p(T)$ data thus obtained have been used to calculate the principal thermodynamic functions of the oxide compound.

Keywords: lutetium gallium titanate, mixed oxide compounds, high-temperature heat capacity, thermodynamic properties

DOI: 10.1134/S0020168520120055

INTRODUCTION

Unfailing interest of researchers and practicians in rare-earth titanates is aroused by their potential practical applications [1–5]. The best studied among them are rare-earth dititanates: $R_2Ti_2O_7$ (R = rare-earth element). Data on their crystal structure have been presented in many reports [1, 6–10]. The $R_2Ti_2O_7$ (R = Sm–Lu, Y) compounds have a cubic face-centered pyrochlore structure (sp. gr. *Fd*3*m*) [6–10], whereas $La_2Ti_2O_7$, $Pr_2Ti_2O_7$, and $Nd_2Ti_2O_7$ crystals have a monoclinic structure (sp. gr. $P2_1$) [1, 11, 12]. There are also published data on their magnetic [1, 12, 13], electrical [1, 14], and dielectric [15] properties. At the same time, many properties of the $R_2Ti_2O_7$ titanates (especially their thermophysical properties) have not yet been studied in sufficient detail. Moreover, $RMTi_2O_7$ (M = Ga, Fe) substituted titanates are essentially unexplored. Such compounds were first obtained by Genkina et al. [16]. They were shown to exist in the systems with R = Sm–Lu and M = Ga and Fe, but not in stannate or zirconate systems and not at M = Cr or Al. In addition, Genkina et al. [16] reported that, in the synthesized series of substituted rare-earth titanates, crystal structure was only determined for $GdGaTi_2O_7$. Note that there are such data for the $RMGe_2O_7$ (M = Al, Ga, In, Fe) substituted germanates [17–19].

The objectives of this work were to determine the crystal structure of the $LuGaTi_2O_7$ titanate, measure the heat capacity of the synthesized samples as a function of temperature in the range 350–1000 K, and evaluate its principal thermodynamic functions from these data.

EXPERIMENTAL

Given the high melting points of its constituent oxides, the $LuGaTi_2O_7$ substituted titanate was prepared by solid-state reaction. For this purpose, after calcination at 1173 K stoichiometric amounts of the starting oxides (extrapure-grade TiO_2 and Ga_2O_3 and reagent-grade Lu_2O_3) were mixed, homogenized by grinding in an agate mortar, and pressed into pellets, which were then sequentially fired in air at 1273 K for 10 h and three times at 1573 K for 5 h. To drive the solid-state reaction to completion, the pellets were reground after each firing step and the resultant powders were then re-pressed. The phase composition of the samples thus prepared was determined by X-ray diffraction. X-ray powder diffraction patterns of $LuGaTi_2O_7$ were collected at room temperature on a

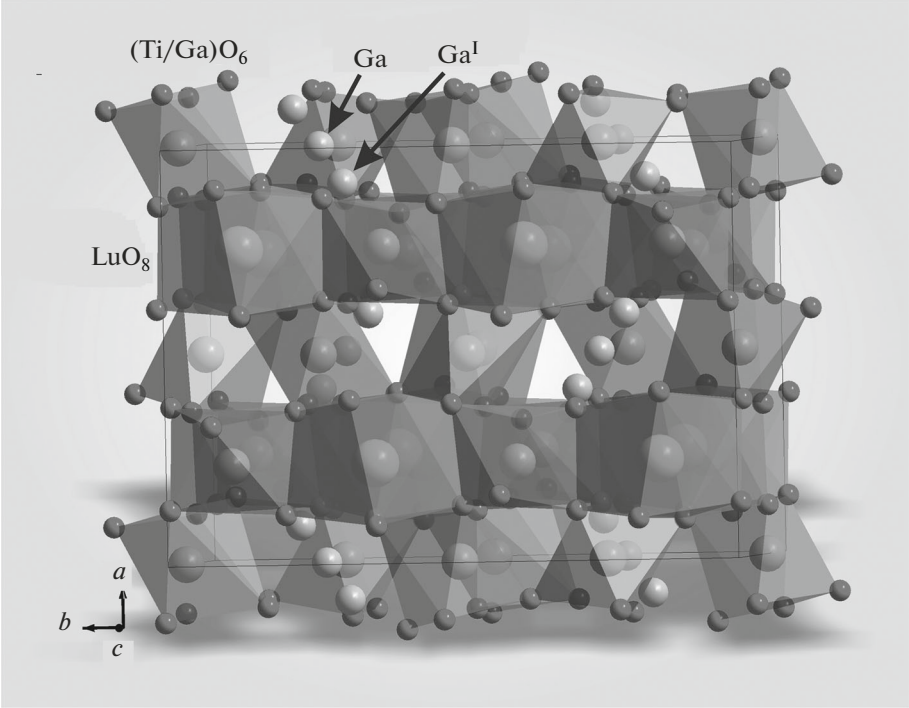

Fig. 1. Crystal structure of $LuGaTi_2O_7$.

Bruker D8 Advance diffractometer (CuK_α radiation) equipped with a VANTEC linear detector. In the X-ray diffraction measurements, we used a 0.6-mm incident beam slit. The angular range was 2θ= 11°–100°, the scan step was maintained constant at 0.016° throughout the angular range, and the counting time per data point was 2 s in each step.

The high-temperature heat capacity C_p of $LuGaTi_2O_7$ was determined by differential scanning calorimetry using an STA 449 C Jupiter thermoanalytical system (Netzsch, Germany). The experimental procedure was described in detail elsewhere [20]. The experimental data were analyzed using the Netzsch Proteus Thermal Analysis software package and licensed Systat Sigma Plot graphing software (Systat Software Inc, the United States). The uncertainty in our measurements was within 2%.

RESULTS AND DISCUSSION

All reflections in X-ray diffraction patterns were indexed in an orthorhombic structure (sp. gr. *Pcnb*) with unit-cell parameters similar to those of $GdGaTi_2O_7$ [16]. Because of this, the crystal structure of this compound was used as an input model for Rietveld refinement with TOPAS 4.2 software [21]. The Gd ions were replaced by Lu ions (Fig. 1). In the structure of $GdGaTi_2O_7$, one Ga ion is disordered in two positions, 4*c* (Ga) and 8*d* (Ga^I), with site occupancies of 0.78 and 0.11, respectively [16]. These data were obtained by structure refinement for single-crystal samples. In this study, we used a powder sample in structure refinement, which was thus less accurate, so the above site occupancies were maintained constant. It is also known from the input model for $GdGaTi_2O_7$ that three sites in an independent part of a cell are occupied by Ti/Ga. The disorder does not include a few sites, unlike in the case of Ga/Ga^I. Because of this, we made an attempt to refine the Ti/Ga site occupancies. To improve refinement stability, a limitation in the form of linear equations was imposed on the total number of Ti and Ga ions per unit cell. As a result, refinements proceeded stably and converged to small agreement parameters (Table 1, Fig. 2). The atomic position coordinates and thermal

Table 1. Principal intensity data collection and structure refinement parameters for a $LuGaTi_2O_7$ crystal (sp. gr. *Pcnb*)

a, Å	9.75033(13)
b, Å	13.46425(17)
c, Å	7.29215(9)
V, Å ^{3}	957.32(2)
d, g/cm^3	6.28
2θ range, deg	11–100
R_{wp}, %	4.78
R_p, %	3.60
R_B, %	0.86
χ^2	2.3

a, *b*, *c*, and β are the unit-cell parameters; *V* is the unit-cell volume; *d* is the calculated density; R_{wp}, R_p, and R_B are the weighted profile, profile, and Bragg agreement factors, respectively; and χ^2 is the goodness-of-fit index.

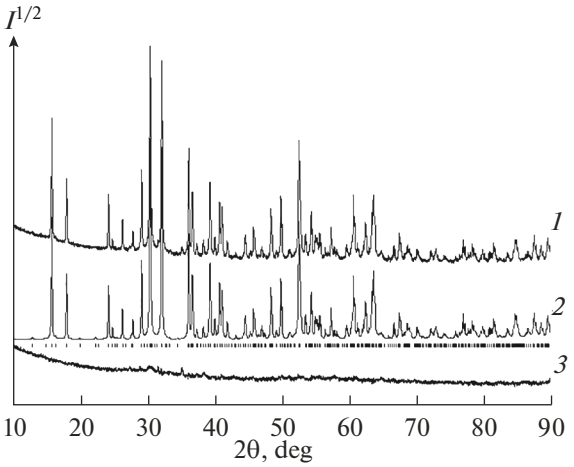

Fig. 2. (*1*) Raw X-ray diffraction data, (*2*) calculated profile, and (*3*) difference plot after refinement by the Rietveld method for $LuGaTi_2O_7$ at room temperature. The vertical tick marks show the calculated positions of allowed reflections.

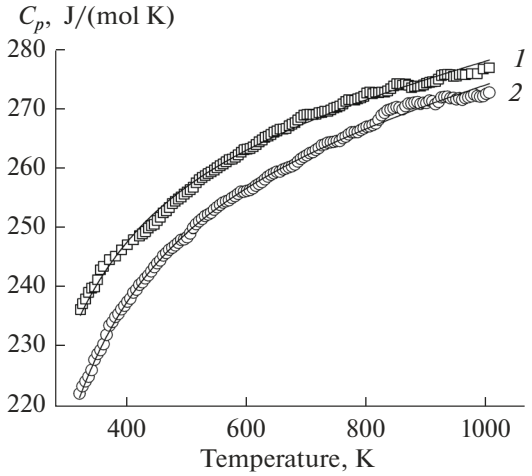

Fig. 3. Temperature dependences of molar heat capacity for (*1*) $Lu_2Ti_2O_7$ and (*2*) $LuGaTi_2O_7$.

parameters are given in Table 2, and the principal bond lengths are listed in Table 3.

Figure 3 and Table 4 present experimental data illustrating the effect of temperature on the heat capacity of $LuGaTi_2O_7$. It is seen that, as the temperature is raised from 320 to 1000 K, its C_p rises systematically, without any extrema in the $C_p(T)$ curve. This can be interpreted as evidence that, in this temperature range, the $LuGaTi_2O_7$ phase undergoes no polymorphic transformations. The present results are well represented by the classic Maier–Kelley equation [22]:

$$C_p = a + bT - cT^{-2}. \quad (1)$$

For $LuGaTi_2O_7$, it has the following form:

$$C_p = (252.43 \pm 0.61) + (25.7 \pm 0.7)\times 10^{-3}T - (39.56 \pm 0.59)\times 10^{5}T^{-2}. \quad (2)$$

The correlation coefficient for Eq. (2) is 0.9989 and the maximum deviation of the data points from the corresponding smoothed curve is 0.65%.

Table 2. Atomic position coordinates and isotropic thermal parameters in the structure of $LuGaTi_2O_7$

Atom	*x*	*y*	*z*	B_{iso}	Occupancy
Lu	0.2474(6)	0.13403(10)	–0.0007(8)	0.56(10)	1
Ti1	0.2542(18)	0.3855(3)	0.505(3)	1.00(15)	0.859(13)
Ga1	0.2542(18)	0.3855(3)	0.505(3)	1.00(15)	0.141(13)
Ti2	0.5	0.25	0.251(2)	1.0(3)	0.808(47)
Ga2	0.5	0.25	0.251(2)	1.0(3)	0.192(47)
Ti3	0.0038(8)	0.4869(4)	0.2505(13)	1.0(2)	0.737(27)
Ga3	0.0038(8)	0.4869(4)	0.2505(13)	1.0(2)	0.263(27)
Ga	0	0.25	0.3305(14)	2.2(3)	0.78
Gai	0.044(5)	0.287(3)	0.171(6)	2.2(3)	0.11
O1	0.1649(10)	0.3936(10)	0.242(5)	0.35(16)	1
O2	0.3951(17)	0.1078(13)	0.252(6)	0.35(16)	1
O3	0.103(2)	0.1537(9)	0.224(3)	0.35(16)	1
O4	0.371(3)	0.286(2)	0.432(3)	0.35(16)	1
O5	0.375(3)	0.277(2)	0.057(4)	0.35(16)	1
O6	0.366(3)	0.497(2)	0.436(4)	0.35(16)	1
O7	0.380(3)	0.487(2)	0.054(4)	0.35(16)	1

Table 3. Principal bond lengths (Å) in the structure of $LuGaTi_2O_7$

Lu–O2	2.37(4)	Ga–O3	1.811(17)
Lu–O2^{I}	2.30(4)	Ga–O5^{IV}	2.08(3)
Lu–O3	2.18(2)	Gai–O1	1.93(5)
Lu–O3^{I}	2.50(2)	Gai–O3	1.93(5)
Lu–O4^{I}	2.40(3)	Gai–O3^{VI}	1.68(5)
Lu–O5	2.33(3)	Gai–O4^{I}	1.93(5)
Lu–O6^{II}	2.21(3)	(Ti2/Ga2)–O4	1.88(3)
Lu–O7^{III}	2.40(3)	(Ti2/Ga2)–O5	1.90(3)
(Ti1/Ga1)–O1	2.11(4)	(Ti3/Ga3)–O1	2.012(13)
(Ti1/Ga1)–O1^{IV}	1.91(4)	(Ti3/Ga3)–O2^{V}	1.903(18)
(Ti1/Ga1)–O4	1.84(3)	(Ti3/Ga3)–O3^{VI}	2.167(15)
(Ti1/Ga1)–O5^{IV}	1.97(3)	(Ti3/Ga3)–O6^{VII}	1.93(3)
(Ti1/Ga1)–O6	1.91(3)	(Ti3/Ga3)–O7^{IV}	2.49(3)
(Ti1/Ga1)–O7^{IV}	1.92(3)	(Ti3/Ga3)–O7^{VII}	1.90(3)
(Ti2/Ga2)–O2	2.171(17)		

Symmetry code: (I) $-x + 1/2, y, z - 1/2$; (II) $-x + 1/2, y - 1/2, -z + 1/2$; (III) $x, y - 1/2, -z$; (IV) $-x + 1/2, y, z + 1/2$; (V) $-x + 1/2, y + 1/2, -z + 1/2$; (VI) $-x, -y + 1/2, z$; (VII) $x - 1/2, -y + 1, -z + 1/2$; (VIII) $x - 1/2, -y + 1/2, z + 1/2$.

Table 4. Thermodynamic properties of $LuGaTi_2O_7$

T, K	C_p, J/(mol K)	$H°(T) - H°(320\ K)$, kJ/mol	$S°(T) - S°(320\ K)$, J/(mol K)	$-(\Delta G°/T)$,* J/(mol K)
320	222.0	–	–	–
350	229.1	6.77	20.22	0.87
400	238.0	18.46	51.43	5.27
450	244.4	30.53	79.85	12.01
500	249.5	42.88	105.9	20.11
550	253.5	55.46	129.8	29.01
600	256.9	68.22	152.0	38.35
650	259.8	81.14	172.7	47.90
700	262.3	94.19	192.1	57.52
750	264.7	107.4	210.3	67.10
800	266.8	120.7	227.4	76.59
850	268.8	134.0	243.6	85.94
900	270.7	147.5	259.1	95.14
950	272.5	161.1	273.7	104.1
1000	274.2	174.8	287.7	113.0

* $-(\Delta G°/T) = (H°(T) - H°(320\ K))/T - (S°(T) - S°(320\ K))$.

Since no heat capacity data for the $LuGaTi_2O_7$ substituted titanate are available in the literature, for comparison Fig. 3 presents heat capacity data for $Lu_2Ti_2O_7$ [23]. It is seen that replacing some of the Lu ions by Ga reduces the heat capacity of the material, but the $C_p(T)$ curves of the two titanates are similar in shape throughout the temperature range studied.

The 298-K heat capacity of $LuGaTi_2O_7$ evaluated using the Neumann–Kopp additive rule [24, 25] is $C_p = 208$ J/(mol K), which differs by 3.5% from the value obtained using Eq. (2). In the calculation by Eq. (2), we used the heat capacities of Lu_2O_3, Ga_2O_3, and TiO_2 borrowed from Leitner et al. [24].

Using the present heat capacity data in the form of Eq. (2) in combination with well-known thermodynamic relations, we evaluated the principal thermodynamic functions of $LuGaTi_2O_7$. The results are presented in Table 4.

CONCLUSIONS

The $LuGaTi_2O_7$ substituted titanate has been prepared by solid-state reaction and its crystal structure has been determined. Its heat capacity has been measured as a function of temperature. The experimental data have been shown to be well represented by the Maier–Kelley equation in the range 320–1000 K. These data have been used to calculate the principal thermodynamic functions of the lutetium gallium titanate.

ACKNOWLEDGMENTS

We are grateful to our colleagues at the Krasnoyarsk Regional Shared Research Facilities Center, Krasnoyarsk Scientific Center (Federal Research Center), Siberian Branch, Russian Academy of Sciences.

REFERENCES

1. Komissarova, L.I., Shatskii, V.M., Pushkina, G.Ya., Shcherbakova, L.G., and Mamsurova, L.G., *Soedineniya redkozemel'nykh elementov. Karbonaty, oksalaty, nitraty, titanaty* (Rare-Earth Compounds: Carbonates, Oxalates, Nitrates, and Titanates), Moscow: Nauka, 1984.
2. Suslov, D.N., Heat capacity and thermal conductivity of dysprosium titanate, *Perspekt. Mater.,* 2004, no. 3, pp. 28–30.
3. Vasil'eva, M.F., Gerasyuk, A.K., Goev, A.I., Potelov, V.V., Senik, B.N., Sukhachev, A.B., Zhigarnovskii, B.M., and Kirilenko, V.V., High-quality optical coatings for the visible and near-IR spectral regions, based on new film-forming materials: gadolinium dititanate and lutetium dititanate, *Prikl. Fiz.,* 2007, no. 5, pp. 91–98.
4. Li, C., Xiang, H., Chen, J., and Fang, L., Phase transition, dielectric relaxation and piezoelectric properties of bismuth doped $La_2Ti_2O_7$ ceramics, *Ceram. Int.,* 2016, vol. 42, pp. 1153–1158.
5. Gao, Z., Liu, L., Han, X., Meng, X., Cao, L., Ma, G., Liu, Y., Yang, J., Xie, Q., and He, H., A ferroelectric ceramic with perovskite-like layered structure (PLS), *J. Am. Ceram. Soc.,* 2015, vol. 98, no. 12, pp. 3930–3934.
6. Portnoi, K.I. and Timofeeva, N.I., *Kislorodnye soedineniya redkozemel'nykh elementov* (Rare-Earth Oxide Compounds), Moscow: Metallurgiya, 1986.
7. Farmer, J.M., Boatner, L.A., Chakoumakos, B.C., Du, M.-H., Lance, M.J., Rawn, C.J., and Bruan, J.C., Structural and crystal chemical properties of rare-earth titanate pyrochlores, *J. Alloys Compd.,* 2014, vol. 605, pp. 63–70. https://doi.org/10.1016/j.jallcom.2014.03.153
8. Liu, C.G., Chen, L.G., Yang, D.Y., Wen, J., Dong, L.Y., and Li, Y.H., The "bimodal effect" of the bulk modulus of rare-earth titanate pyrochlore, *Comp. Mater. Sci.,* 2016, vol. 114, pp. 233–235. https://doi.org/10.1016/j.commatsci.2015.12.024
9. Zhang, W., Zhang, L., Zong, H., Li, L., Yang, X., and Wang, X., Synthesis and characterization of ultrafine $Ln_2Ti_2O_7$ (Ln = Sm, Gd, Dy, Er) pyrochlore oxides by stearic method, *Mater. Character.,* 2010, vol. 61, pp. 154–158. https://doi.org/10.1016/j.materchar.2009.11.005
10. Baraudi, K., Gaulin, B.D., Lapidus, S.H., Gaudet, J., and Cava, R.J., Symmetry and light stuffing of $Ho_2Ti_2O_7$, $Er_2Ti_2O_7$, and $Yb_2Ti_2O_7$ characterized by synchrotron X-ray diffraction, *Phys. Rev. B: Condens. Matter Mater. Phys.,* 2015, vol. 92, paper 024110. https://doi.org/PhysRevB.92.024110
11. Hwang, D.W., Lee, J.S., Li, W., and Oh, S.H., Electronic band structure and photocatalytic activity of $Ln_2Ti_2O_7$ (Ln = La, Pr, Nd), *J. Phys. Chem. B,* 2003, vol. 107, pp. 4963–4970. https://doi.org/10.1021/jp034229n
12. Xing, H., Long, G., Guo, H., Zou, Y., Feng, C., Cao, G., Zeng, H., and Xu, Z.-A., Anisotropic paramagnetism of monoclinic $Nd_2Ti_2O_7$ single crystals, *J. Phys.: Condens. Matter,* 2011, vol. 23, paper 216005. https://doi.org/10.1088/0953-8984/23/21/216005
13. Ben Amor, N., Bejar, M., Hussein, M., Dhahri, E., Valente, M.A., and Hlil, E.K., Synthesis, magnetic properties, magnetic entropy and Arrot plot of antiferromagnetic frustrated $Er_2Ti_2O_7$ compound, *Supercond. Nov. Magn.,* 2012, vol. 25, pp. 1035–1042. https://doi.org/10.1007/s10948-011-1344-9
14. Gao, Z., Wu, L., Gu, W., Zhang, T., Liu, G., Xie, Q., and Li, M., The anisotropic conductivity of ferroelectric $La_2Ti_2O_7$ ceramics, *J. Eur. Ceram. Soc.,* 2017, vol. 37, no. 1, pp. 137–143. https://doi.org/10.1016/j.jeurceramsoc.2016.08.020
15. Gao, Z., Shi, B., Ye, H., Yan, H., and Reece, M., Ferroelectric and dielectric properties of $Nd_{2-x}Ce_xTi_2O_7$ ceramics, *Adv. Appl. Ceram.,* 2014, vol. 144, no. 4, pp. 191–197. https://doi.org/10.1179/1743676114Y.0000000221
16. Genkina E.A., Adrianov I.I., Belokoneva E.A., Mill' B.V., Maksimov B.A., and Tamazyan, R.A., Synthetic $GdGaTi_2O_7$: a new polymorph of polymignite, *Kristallografiya,* 1991, vol. 36, no. 9, pp. 1408–1414.
17. Jarchow, O., Klaska, K.-H., and Schenk-Strauß, H., Die Kristallstructuren von $NdAlGe_2O_7$ und $NdGaGe_2O_7$, *Z. Kristallogr.,* 1985, vol. 172, pp. 159–166.
18. Kaminskii, A.A., Mill, B.V., Butashin, A.V., Belokoneva, E.L., and Kurbanov, K., Germanates with $NdAlGe_2O_7$-type structure, *Phys. Status Solidi A,* 1987, vol. 103, pp. 575–582.
19. Juarez-Arellano, E.A., Campa-Molina, J., Ulloa-Godinez, S., Bucio, L., and Orozco, E., Crystallochemistry of thortveitite-like and thortveitite-type compounds, *Mater. Res. Soc. Symp. Proc.,* 2005, vol. 848, pp. FF6.15.1–FF6.15.8.
20. Denisova, L.T., Irtyugo, L.A., Kargin, Yu.F., et al., High-temperature heat capacity and thermodynamic properties of $Tb_2Sn_2O_7$, *Inorg. Mater.,* 2017, vol. 53, no. 1, pp. 93–95. https://doi.org/10.1134/S0020168517010046

21. *Bruker AXS TOPAS V4: General Profile and Structure Analysis Software for Powder Diffraction Data – User's Manual,* Karlsruhe: Bruker AXS, 2008.

22. Maier, C.G. and Kelley, K.K., An equation for the representation of high temperature heat content data, *J. Am. Chem. Soc.,* 1932, vol. 54, pp. 3243–3246. https://doi.org/10.1021/ja01347a029

23. Denisova, L.T., Chumilina, L.G., Ryabov, V.V., Kargin, Yu.F., Belousova, N.V., and Denisov, V.M., Heat capacity of the $Gd_2Ti_2O_7$ and $Lu_2Ti_2O_7$ pyrochlores in the range 350–1000 K, *Inorg. Mater.,* 2019, vol. 55, no. 5, pp. 477–481. https://doi.org/10.1134/S0020168519050029

24. Leitner, J., Chuchvalec, P., Sedmidubský, D., Strejc, A., and Abrman, P., Estimation of heat capacities of solid mixed oxides, *Thermochim. Acta,* 2003, vol. 395, pp. 27–46. https://doi.org/10.1016/S0040-6031(02)00176-6

25. Leitner, J., Voňka, P., Sedmidubský, D., and Svoboda, P., Application of Neumann–Kopp rule for the estimation of heat capacity of mixed oxides, *Thermochim. Acta,* 2010, vol. 497, pp. 7–13. https://doi.org/10.1016/j.tca.2009.08.002

Translated by O. Tsarev